

Computational modelling of slag foaming in pyrometallurgical furnaces

Quinn G. Reynolds*, Markus W. Erwee

Pyrometallurgy Division, Mintek, Private Bag X3015, Randburg 2125

quinnr@mintek.co.za

ABSTRACT

In pyrometallurgical furnaces, raw materials are processed into products of value at high operating temperatures (1500°C or more). The materials are typically in a molten state, and will separate into two or more immiscible liquid phases due to differences in chemical composition. One such phase is slag, which contains predominantly metal oxides and is generally the least dense of the liquid phases present. Expansion and foaming of the slag layer is occasionally observed during furnace operation, and occurs as a result of the injection or generation of gases in the molten bath. Uncontrolled slag foaming may cause damage to the furnace interior or, in extreme cases, catastrophic failure. Controlled slag foaming can however be used to great effect in limiting energy losses from furnaces and improving their thermal efficiency.

A computational modelling study of gas passing through a slag layer using the OpenFOAM[®] platform is presented. Existing multiphase fluid flow solvers based on the volume of fluids (VOF) method were extended and used to model the influence of operating conditions and material properties on the extent and nature of slag foaming. The resulting model was successfully validated against empirical data and correlations from literature. A dimensional analysis was conducted on the slag foaming problem, and the effect of various key dimensionless groups on the computational model was studied.

KEYWORDS

Pyrometallurgy, Multiphase, Foaming

INTRODUCTION

The discipline of pyrometallurgy deals with the treatment of raw materials at high temperatures in order to create products of increased value. Pyrometallurgical furnaces are used extensively for the production and recycling of many commodities including iron and steel, ferro-alloys, titanium dioxide, platinum group metals, and others (Jones and Curr [1]). Because of the very high operating temperatures, the process materials inside furnaces are generally in the molten state, and typically separate into two immiscible phases, slag and metal. The slag phase contains predominantly metal oxides and generally floats above the denser metal phase.

Furnace processes may be classified in many ways, including but not limited to whether any chemical reactions are utilised to convert feed materials from one form to another (melting vs smelting), and whether or not the molten bath of process material inside the vessel is exposed to the gas atmosphere (open-bath) or covered by a layer of solid feed material (closed-bath). Some examples in the case of direct-current electric furnaces are shown in Figure 1. In the present study, only open-bath smelting furnaces are considered.

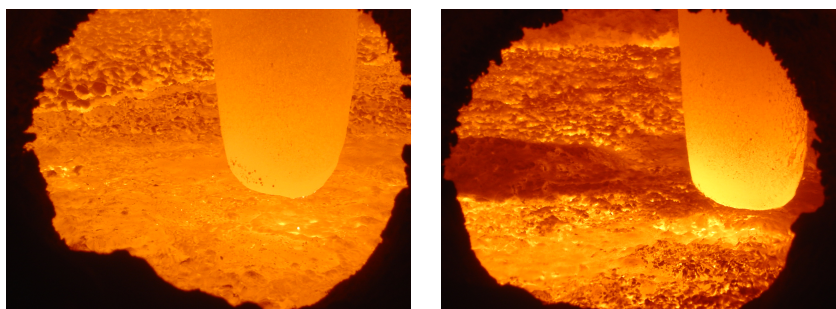


Figure 1. DC pilot-scale furnace interior, open bath (left) and partially closed bath (right) conditions

During the chemical reactions occurring in smelting furnaces, which typically involve the reaction of metal oxides with a carbonaceous reductant to produce metal products, gases such as carbon monoxide are evolved. Depending on the mechanism of the reduction reactions, the gas may be generated at the contact surfaces between solid reductant particles and molten slag (which in general are dispersed throughout the slag layer), or at the interface between the metal and slag liquid phases. The generated gas forms bubbles and rises through the slag in order to leave the furnace vessel causing the molten slag layer to be partially displaced and increasing its effective thickness. If the displacement is appreciable, this process is referred to as slag foaming.

Slag foaming is very much a double-edged sword for furnace operations – if it can be managed and controlled, the foamy layer of slag can help to shield the hot bath surface and coat the walls and roof of the furnace, reducing energy losses and protecting the refractory materials lining the vessel. If however uncontrolled foaming events occur, they can lead to increased wear and damage to the refractories and ultimately to premature furnace failure. Understanding slag foaming as it relates to a given process is therefore of considerable value to furnace operators.

Slag foaming behaviour is generally grouped into two distinct phenomena – expanded slags and true foaming. In slag expansion, the slag layer increases in thickness primarily as a result of the time taken for the gas bubbles to rise through it. In true foaming, the slag layer thickness increases primarily as a result of the formation of a layer of bubbles with high void fraction which accumulates near the slag surface. The difference is illustrated in Figure 2.

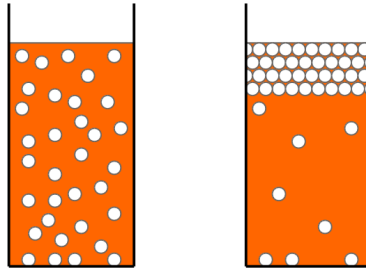


Figure 2. Comparison of slag expansion (left) and true foaming (right)

In real furnace systems the distinction between true foaming and expanded slags is often somewhat academic. Expansion is in general associated with higher and true foaming with lower gas flowrates (Seetharaman et al [2]), but it is quite possible for both phenomena to be occurring to some degree at the same time (Ozturk and Fruehan [3]). In the present paper however, the focus is on true slag foaming phenomena and the development of possible methods to model them.

One indicator of how likely a particular metallurgical slag is to generate a foam layer is the slag foaming index Σ , which has units of time and is defined as the rate of change of the foam layer thickness H_f with superficial gas velocity (Seetharaman et al [2]). Several authors have raised concerns over the use of the slag foaming index as a variable (Lotun and Pilon [4]), however, it remains valuable as a guidance tool for many industrial furnace operations where foaming occurs. A number of experimental studies of the effect of changing various parameters of interest on the slag foaming index have been performed; much of this body of earlier work also presents the results of dimensional analyses of the slag foaming problem, and empirical relationships between the dimensionless groups identified. Some examples are shown below (see Table 1 for definitions of the symbols used; the K_i are constants fitted from experimental data).

$$\Sigma = K_1 \frac{\mu}{\sqrt{\rho\sigma}} \quad (\text{Jiang and Fruehan [5]}) \quad (1)$$

$$\Sigma = K_2 \frac{\mu^{1.2}}{\rho\sigma^{0.2}d_b^{0.9}} \quad (\text{Zhang and Fruehan [6]}) \quad (2)$$

$$\Sigma = K_3 \frac{\mu^{0.8}}{(\rho\sigma)^{0.8}d_b^{2.6}u_g^{0.2}} \quad (\text{Pilon et al [7], assuming zero minimum foaming velocity}) \quad (3)$$

Although there is considerable variation in the exact values of the powers and empirical constants, the degree to which a slag is prone to foaming is generally proportional to the slag's viscosity, and inversely proportional to its density, surface tension, and the diameter of the gas bubbles.

Following the general approach of Pilon et al [7] but retaining the slag foaming index, the parameters shown in Table 1 are identified in relation to the slag foaming problem. It is assumed that the gas phase density and viscosity are low relative to the slag, and have comparatively little effect on bubble and foam behaviour.

Table 1. Variables of interest in slag foaming

Slag density	ρ , kg/m ³	Bubble diameter	d_b , m
Slag viscosity	μ , Pa.s	Interfacial surface tension	σ , N/m
Superficial gas velocity	u_g , m/s	Gravitational acceleration	g , m/s ²
Slag foaming index	$\frac{dH_f}{du_g} = \Sigma$, s		

Dimensional analysis using these variables yields the following functional relationship between four dimensionless groups:

$$N_{\Sigma} = \frac{g\mu\Sigma}{\sigma} = f(N_{Mo}, N_{Ca}, N_{Ar}) \quad (4a)$$

$$N_{Mo} = \frac{g\mu^4}{\rho\sigma^3} \quad (4b)$$

$$N_{Ca} = \frac{\mu u_g}{\sigma} \quad (4c)$$

$$N_{Ar} = \frac{g\rho^2 d_b^3}{\mu^2} \quad (4d)$$

Here, N_{Mo} is the Morton number, N_{Ca} the Capillary number, and N_{Ar} the Archimedes number. The effect of these groups in determining the functional dependence in (4a) will be studied further during the course of the paper.

To date, it would appear that little work has been performed in the field of computational modelling of slag foaming. This can be attributed to the success of theoretical and empirical correlations such as (1) – (3) and others in indicating foam formation within narrow parameter ranges for particular processes. Another contributing factor is that for design purposes, there is generally more interest in modelling the effects of foaming at the scale of industrial furnaces (tens of meters) rather than at the scale of the gas bubbles in the slag (a few millimeters). The foam layer is therefore often completely ignored in computational models, or treated in an approximated manner – for example as a continuum phase requiring considerable empirical input into the calculation (Sattar et al [8]), or using Euler-Lagrange-type formulations which represent bubbles or groups of bubbles as individual particles of a set shape, usually spherical (Lain et al [9]). Although they have great engineering utility, such approaches are not entirely satisfactory for a more fundamental exploration of slag foam formation and evolution at smaller scales.

MODEL DESCRIPTION

In order to study foaming phenomena in slags, a computational solver was implemented using the OpenFOAM[®] open source framework (OpenFOAM [10]). An existing volume-of-fluids (VOF) based multiphase flow solver was extended and enhanced for this purpose.

Several interesting challenges arise when attempting to model bubble phenomena using VOF methods. Perhaps the most important is the large difference in scale between the bubbles, which are typically a few millimeters in diameter in the slag foaming case, and the interfacial films between them, which may be as little as a few nanometers in thickness. As the VOF method can by definition only model an interface between phase fields which is of the order of the mesh resolution and no sharper, direct simulation of the film would require excessively fine and computationally-expensive meshes. If coarser meshes are used, particularly with materials such as slags having high surface tension, film structures in models using this

method rupture prematurely – this makes VOF unsuitable in its standard form for modelling phenomena such as foams.

The aim of the present solver was to address some aspects of this problem in order to permit direct modelling of slag foam dynamics. To this end, the following modifications to the multiphaseInterFoam solver in OpenFOAM® were made:

- Each bubble in the model is treated as a separate phase, with each of these phases having physical properties identical to the main gas phase. Interfacial surface tension between the bubble phases is set at double the surface tension between the slag and gas phases to approximate the presence of a double-walled film of slag.
- A bubble bursting algorithm based on a film drainage sub-model was implemented. This involves testing of the interfaces between all pairs of bubble phases in the model at each time step. If the two phases are in sufficiently direct contact with each other, the film thickness between each of the involved phases is calculated using a film drainage sub-model. Once the film thickness for a particular bubble phase drops below a specified value (the minimum stable film thickness), and if the phase concerned is in contact with the main gas atmosphere, the bubble is burst by sweeping the model region, adding the bubble phase fraction to the main gas phase fraction, and setting the bubble phase fraction to zero. This has the effect of instantaneously removing the film separating this particular bubble from the main gas atmosphere, and merging its contents with the surrounding gas phase.
- By way of example a relatively simple film drainage sub-model based on flow driven by gravitational and capillary forces was implemented, and relates the film drainage time to the density, viscosity and surface tension of the slag as well as a representative scale measure calculated from the film perimeter length at every time step. Considerably more sophisticated approaches based on theoretical and experimental treatments of thin films (Bazilekhov et al [11], Chan et al [12]) are possible, and may be integrated into the present framework in a similar way.

As part of the standard multiphaseInterFoam solver algorithm, the VOF method is used to take account of the phase separation, requiring solution of a separate convective transport equation for the volume fraction field of each phase. This permits the use of a single velocity and pressure field to describe all phases in the multiphase system. The Pressure Implicit with Splitting of Operators (PISO) predictor-corrector algorithm is used for calculation of the flow fields at each time step. Gradient-limited discretisations were used for all divergence terms with the exception of those related to the phase fraction fields, for which the van Leer compression scheme together with the Multidimensional Universal Limiter for Explicit Solution (MULES) solution algorithm was specified. Adaptive time stepping was applied to keep the mesh Courant number below 0.75 in order to ensure acceptable numerical stability.

Film Sub-Model

The film sub-model was developed from the work of Nguyen et al [13] on the drainage of liquid magma from the films around gaseous bubbles at the surface of the melt. Two relationships are given for the drainage time, derived from the equations of fluid flow within the film:

$$\frac{d\delta}{dt} = -\frac{1}{C_g} \frac{\rho g d_b}{\mu} \delta \quad (5a)$$

$$\frac{d\delta}{dt} = -\frac{1}{C_c} \frac{\sigma}{\mu d_b} \delta \quad (5b)$$

(5a) describes film drainage due to gravitational effects, and (5b) describes film drainage as a result of capillary pressure. Here, δ is the film thickness, and C_g and C_c are constants independent of the fluid properties and bubble geometry (C_g/C_c is given as 0.25). Combining (5) and integrating gives a relationship for the evolution of the film thickness used in the sub-model:

$$\frac{\delta}{\delta_0} = \exp\left(-\frac{1}{C_g} \left(\frac{\rho g d_b}{\mu} + \frac{C_g}{C_c} \frac{\sigma}{\mu d_b}\right) t\right) \quad (6)$$

(6) is used to track the film thickness for each bubble phase in the slag foaming model over time after activation of the film sub-model. Once the film thickness drops below a certain critical value, bursting of the bubble phase into the main gas phase is triggered.

Geometry and Boundary Conditions

At present only two-dimensional models are considered – although the solver is capable of working in three dimensions, this is computationally expensive and is expected to be of value only once the model’s robustness and quantitative accuracy have been more firmly established.

The model region is a simple rectangular vessel, with one or more injection ports at the base through which the gas to form the bubbles is introduced. A diagram of the region showing the various phase fields and boundaries is shown in Figure 3.

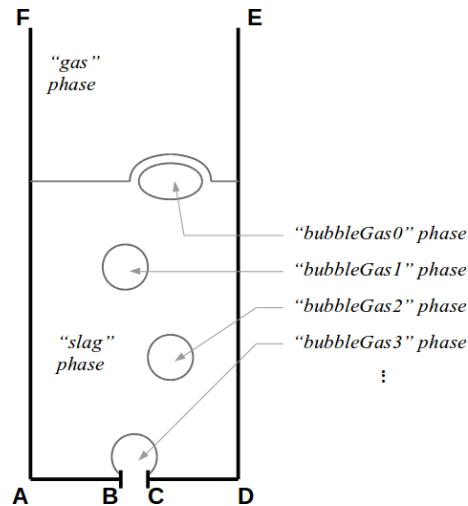


Figure 3. Diagram of model region

The following boundary conditions are applied at the perimeter of the region: FAB and CDE are treated as solid walls, with velocity set to zero and zero pressure gradient. The gradient of all phase fields is also assumed to be zero at these surfaces (equivalent to a wetting angle of 90°). EF is assumed open to atmosphere, at a specified pressure and a velocity calculated from the pressure field. The phase fields are subject to an inlet-outlet condition depending on the direction of flow – zero gradient if outflow, and a gas phase fraction of 1 if inflow. Finally, at boundary BC an intermittent inflow condition is specified, with a fixed velocity for short, regularly-spaced periods to inject bubbles of fixed size at a known average flowrate. During each injection period, the phase fractions of the various bubble phases at this boundary are modulated to ensure that each phase is injected as a separate bubble.

Model performance

Model runs were executed using a combination of local cluster resources (Intel i7 quad-core machines over gigabit ethernet) and nodes of the Lengau machine at the Centre for High Performance Computing. Each model run made use of up to 16 processor cores, however, parallel scaling was generally observed to start falling away from linear at around 8 cores or more due to the relatively small size of the 2D models (this is expected to improve significantly in 3D). Coarse-grained parallelism was employed during the parameter space studies by running multiple model cases simultaneously, with each case using four processors to ensure maximum computational efficiency. Under these conditions, run times of between 16 and 24 hours for a model time of 5 s were typical.

MODEL VALIDATION

The accuracy and validity of the results from the computational model were analysed using an experimental case from slag foaming literature (Ozturk and Fruehan [3]).

The assumed composition of the slag was 48% CaO, 10% FeO, 32% SiO₂ and 10% Al₂O₃ (by mass). Properties were calculated at 1773 K. The effect of a small amount of precipitated solid slag were ignored for all calculations, since the composition of the liquid portion of the slag does not differ significantly from the

bulk composition. The viscosity of the slag was estimated using the ‘Viscosity’ module of FactSage™ (Bale et al [14]), and surface tension and density were calculated based on empirical methods (Mills et al [15]). For the Mills-Keene method, the molar volumes for each of the slag components were taken from Mills et al [16]. Properties of the gas, assumed to be 100% CO at 1773 K, were estimated using ideal gas law relationships. The parameters used in the model are shown in Table 2. Dimensions were chosen to match the size of the crucibles and the gas injection depth used in Ozturk and Fruehan [3].

In the first set of tests, the model’s dependence on the resolution of the computational mesh was examined. A value of 20 s was assumed for the constant C_g in the film sub-model. A single gas bubble was injected at the base of the slag layer at the beginning of each simulation, and the upper position of the slag surface on the region center-line was recorded over time. The results are shown in Figure 4 and Figure 5.

Table 2. Model parameters used in validation and testing

ρ	1990 kg/m ³	Gas density, ρ_g	0.192 kg/m ³
μ	0.1407 Pa.s	Gas viscosity, μ_g	5.64×10^{-5} Pa.s
σ	0.509 N/m	d_b	0.005 m
Initial film δ	10^{-6} m	Critical film δ	10^{-8} m
Region width	0.020 m	Initial slag height	0.037 m

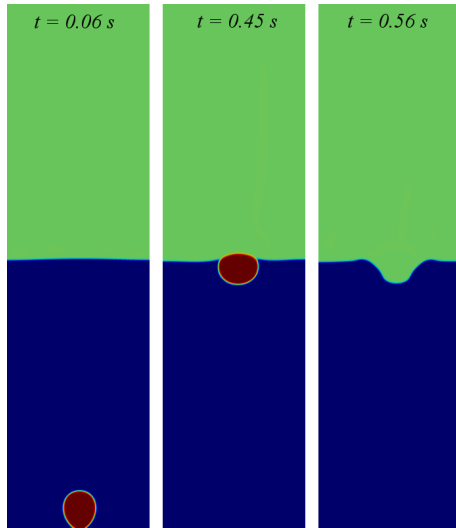


Figure 4. Phase field at various times for mesh resolution 1.67×10^{-4} m

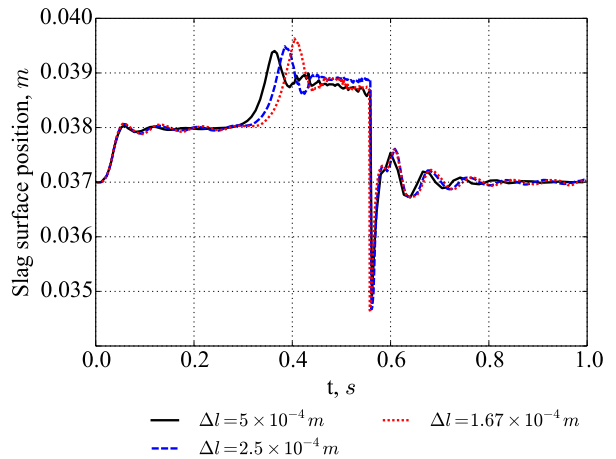


Figure 5. Evolution of slag surface at different mesh resolutions

In general the slag foaming model scales well with mesh resolution, producing relatively similar results even on very coarse meshes. In particular, the time taken for the bubble to burst after it reaches the surface is repeatable across a range of mesh sizes, suggesting that foam behaviour will be captured with reasonable accuracy.

In the second set of tests, a value for C_g was estimated using experimental slag foaming index measurements (Ozturk and Fruehan [3]) from which $\Sigma \approx 0.96$ s at 1773 K. C_g was fitted by comparing the simulated foam height with the experimental data at a fixed superficial gas velocity of 1 cm/s, giving a value of 84.5 s. The gas velocity was then varied to test if the model correctly captures the expected response of the foam height. In all cases 30 different bubble phases were used, and a total model time of 5 s was simulated. Unless otherwise indicated, the model region was meshed at a resolution of 3.3×10^{-4} m.

Foam height was calculated from the model data as the difference between the lowest extremity of the ‘‘gas’’ phase and the highest extremity of the ‘‘slag’’ phase along a selection of vertical line samples taken through the domain at various times. The resulting time series of instantaneous foam heights were averaged over the second half of the 5 s time period to give an indication of the steady-state foam height.

Figure 6 and Figure 7 show results from the slag foaming model running at lower and higher gas flowrates. The foam layer that is formed at the slag surface is visibly thicker in the case of higher gas flowrates, as would be expected from the theory of slag foaming. The calculated average foam heights are compared in Table 3.

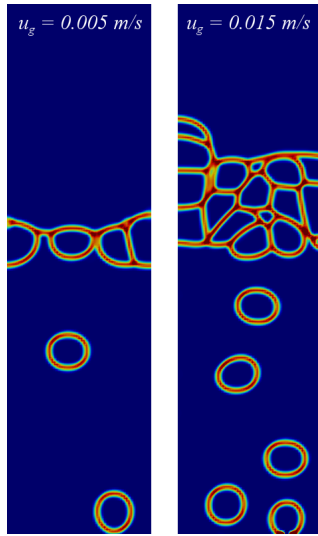


Figure 6. Phase field boundaries for different superficial gas velocities

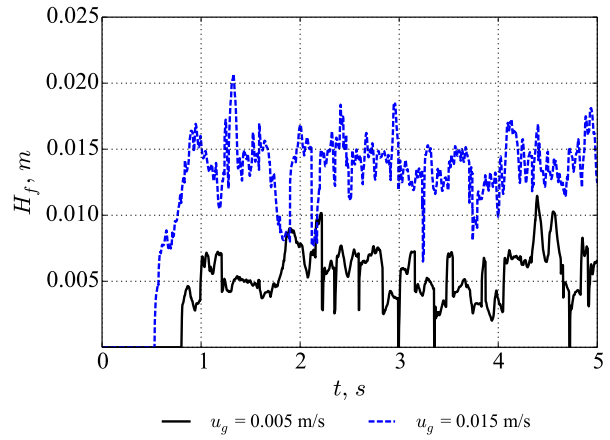


Figure 7. Evolution of foam thickness for different superficial gas velocities

Table 3. Response of computational model to superficial gas velocity

u_g	H_f (theoretical with $\Sigma = 0.96$ s)	H_f (computational model)
0.005 m/s	0.0048 m	0.0055 m
0.015 m/s	0.0144 m	0.0138 m

In both cases, the computational model predicts foam heights within a few percent of the theoretical value assuming a constant value of the slag foaming index. The slight inverse dependence of Σ on u_g observed in the modelling results may also be physically realistic in light of empirical correlations such as (3).

RESULTS AND DISCUSSION

In order to examine the effect of various parameters on the behaviour of the slag foaming model, a base case set of conditions was first identified based on typical average values for a wide range of different slag materials (Mills et al [15], Mills et al [16]). These are shown in Table 4 (other model parameters are as indicated in Table 2).

Table 4. Model parameters for base case

ρ	3000 kg/m ³	σ	0.25 N/m
μ	0.2 Pa.s	d_b	0.005 m
u_g	0.01 m/s	C_g	84.5 s

Results from the base case model are shown in Figure 8 and Figure 9. The slag layer in the model is seen to grow from zero thickness initially while the bubbles rise through the slag to reach the gas interface. Formation of foam is then rapid, and the thickness of the foam layer stabilises at slightly over 10 mm after approximately 1.5 s.

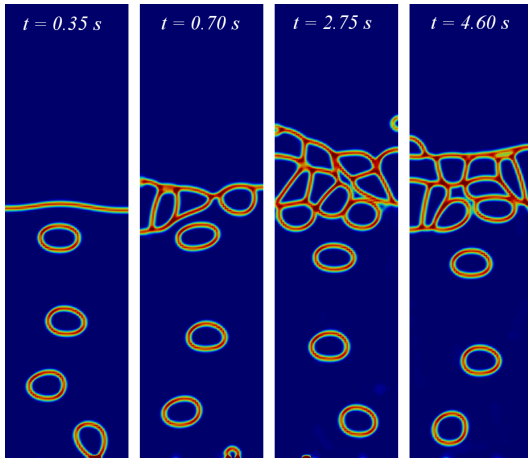


Figure 8. Phase field boundaries at different times, base case

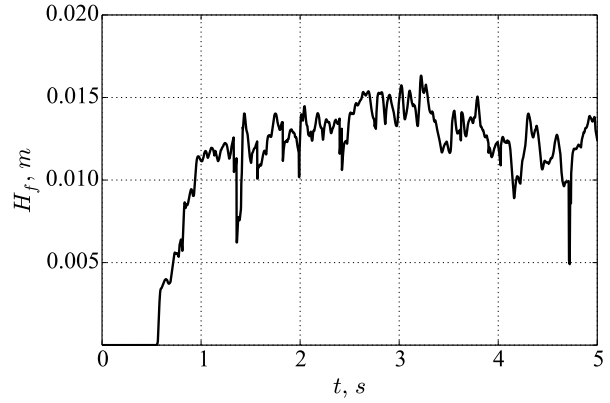


Figure 9. Evolution of foam thickness over time, base case

From the time-averaged value of the foam thickness (0.0130 m), the slag foaming index was determined as 1.30 s for the base case set of parameters.

Response of the model to primitive variables

The response of the computational model's prediction of slag foaming behaviour to changes in primitive variables used to describe the slag properties and operating conditions was tested. Several of the parameters shown in Table 4 were altered one by one while keeping all other variables constant, and the effect on the nature and degree of slag foaming was studied. The results in terms of the slag foaming index are shown in Table 5.

Table 5. Effect of primitive variables on modelled value of Σ

<i>Parameter variation</i>	Σ (<i>model</i>)
Base Case	1.30 s
$\mu = 0.4$ Pa.s	2.56 s
$\sigma = 0.125$ N/m	1.71 s
$\rho = 1500$ kg/m ³	1.81 s
$d_b = 0.004$ m	1.38 s
$d_b = 0.006$ m	1.17 s

It can be seen that doubling the slag viscosity has the most significant impact on the slag foaming index. Halving the surface tension results in a moderate increase in the index relative to the base case, and halving of slag density has a similar effect. The model is considerably less sensitive to bubble diameter, but a slight trend of foaming index increasing with decreasing bubble diameter is observed. Overall, the functional dependence of the computational model matches well with one of the most common forms of empirical model, that shown in equation (1).

Selected visualisations of the phase field boundaries for two of the cases are shown in Figure 10 and Figure 11. The entrainment of the slag phase into the foam layer at different bubble sizes is shown in Figure 12.

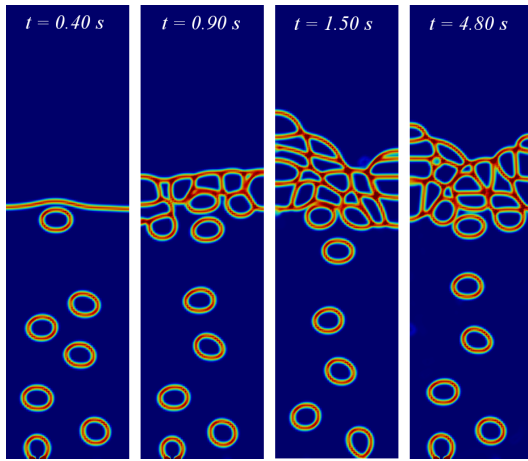


Figure 10. Phase field boundaries at different times for $d_b = 0.004$ m

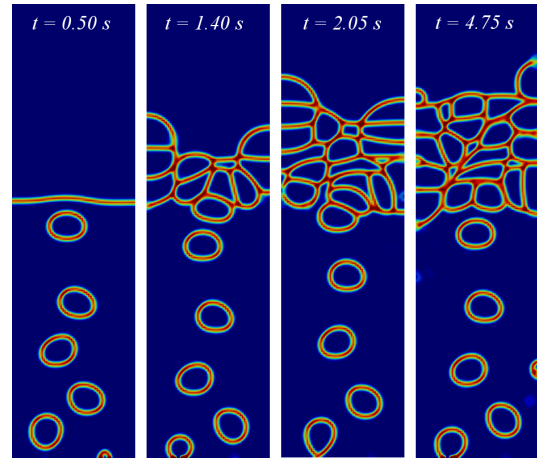


Figure 11. Phase field boundaries at different times for $\mu = 0.4$ Pa.s

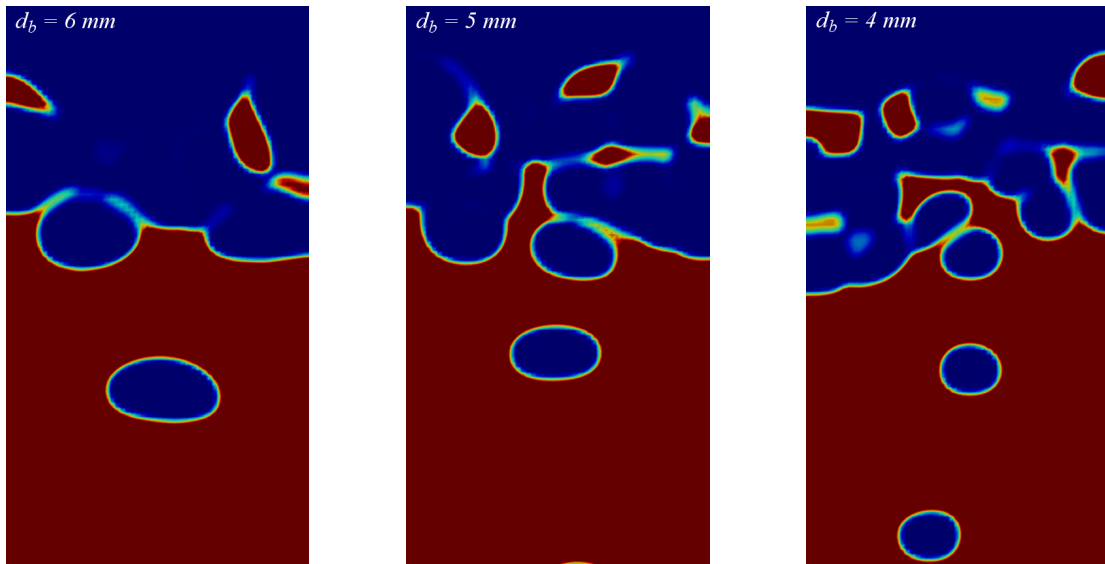


Figure 12. Close-ups of foam layer at end of simulation showing slag phase fraction (blue = 0, red = 1) at different bubble diameters

Smaller bubbles are seen to hold up more of the slag phase in the spaces between them, keeping the film between bubbles “wet” and increasing the lifetime of the foam. Similarly in the case of higher slag viscosity, drainage from the films (controlled predominantly by the film sub-model in use) is substantially slowed when viscosity increases, increasing the time taken before film rupture. As a result, the foam layer thickness at a set gas flowrate is larger, producing a higher slag foaming index.

Response of the model to dimensionless variables

In order to study the dependence of the computational model on the dimensionless groups defined in equation (4), several of the slag parameters were altered simultaneously so as to keep all but one of the dimensionless groups constant. For the base case set of parameters in Table 4, $N_{M0} = 3.35 \times 10^{-4}$, $N_{Ca} = 8.00 \times 10^{-3}$, and $N_{Ar} = 276$.

Six additional cases were set up by multiplying or dividing the value of each of the dimensionless groups by two while keeping the others constant. The average steady-state height of the foam layer generated by the computational model was then estimated and used to determine the slag foaming index as before, allowing the value of the foam index group N_2 to be calculated. Results are shown in Figure 13 and Figure 14.

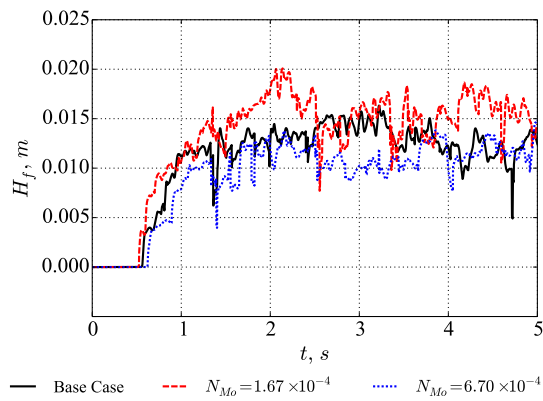


Figure 13. Evolution of slag foam height at different values of N_{Mo}

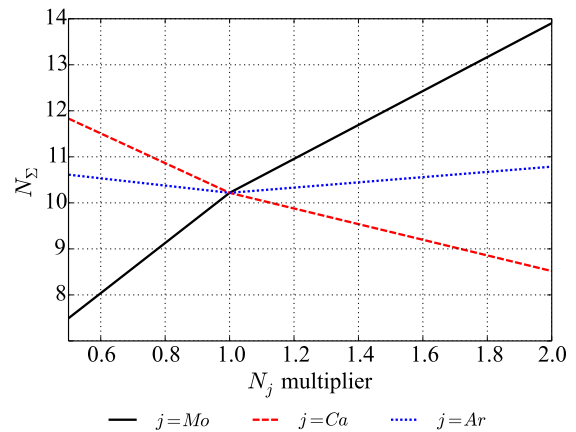


Figure 14. Sensitivity of equation (4) to dimensionless quantities

It was found that N_{Σ} depends strongly on N_{Mo} (increasing as N_{Mo} increases) and N_{Ca} (decreasing as N_{Ca} increases). Relatively little dependence on N_{Ar} was observed in the range of values tested. This behaviour is in agreement with the results from the primitive variable cases which indicated a strong dependence of Σ on μ , which affects predominantly N_{Mo} , and a much weaker dependence on d_b , which affects predominantly N_{Ar} .

CONCLUSIONS

A computational model was successfully developed to study the problem of slag foaming. Simple extensions of standard volume-of-fluid solvers permitted the inclusion of film drainage models and bubble film rupture dynamics to accurately capture the evolution and behaviour of the foam layer. The model was found to be relatively mesh-independent, and was successfully validated against experimental data.

The sensitivity of the computational model's predictions of slag foaming index to variations in slag physical properties and operating conditions was studied. The results were found to match well with empirical correlations of a form commonly used in the smelting industry, in which foaming index is proportional to slag viscosity and inversely proportional to the square root of slag density and surface tension. In addition, the response of the model to changes in various dimensionless groups used to characterise slag foaming was examined, with the Morton and Capillary numbers found to have the largest effect on foaming behaviour.

Much further work is possible in this area. The computational efficiency of the slag foaming model as currently implemented is rather poor, and scales with the number of bubble phases included – a more elegant reformulation of the multiphase bubble flow algorithm would therefore be of value. In addition, the model suffers from the effects of parasitic currents at the bubble phase interfaces, exacerbated in the case of slag foaming problems by the very high interfacial surface tension and very low gas density. Implementation of improved interface-compression methods such as HiRAC (Oxtoby et al [17]) or similar should be investigated as a means of mitigating this issue.

With the alleviation of numerical performance limitations and further validation against experimental data, it is believed that computational models similar to those presented here could potentially become viable alternatives to laboratory testing for estimation of slag foaming behaviour in pyrometallurgical furnaces.

ACKNOWLEDGEMENTS

This paper is published by permission of Mintek. The authors also gratefully acknowledge support from the Centre for High Performance Computing (CHPC).

REFERENCES

- 1 Jones, R.T., and Curr, T.R., "Pyrometallurgy at Mintek", SAIMM Southern African Pyrometallurgy 2006, Johannesburg, South Africa, 2006.
- 2 Seetharaman, S., McLean, A., Guthrie, R., and Sridhar, S., "Treatise on Process Metallurgy Volume 2 (Process Phenomena)", Elsevier, Oxford, United Kingdom, 2014.

- 3 Ozturk, B., and Fruehan, R.J., “Effect of Temperature on Slag Foaming”, *Metallurgical and Materials Transactions B*, Vol. 26B, pp 1086 – 1088, 1995.
- 4 Lotun, D., and Pilon, L., “Physical Modeling of Slag Foaming for Various Operating Conditions and Slag Compositions”, *ISIJ International*, Vol. 45, No.6, pp. 835 – 840, 2005.
- 5 Jiang, R., and Fruehan, R.J., “Slag Foaming in Bath Smelting”, *Metallurgical and Materials Transactions B*, Vol. 22B, pp. 481 – 489, 1991.
- 6 Zhang, Y., and Fruehan, R.J., “Effect of the Bubble Size and Chemical Reactions on Slag Foaming”, *Metallurgical and Materials Transactions B*, Vol. 26B, pp. 803 – 812, 1995.
- 7 Pilon, L., Fedorov, A.G., and Viskanta, R., “Steady-State Thickness of Liquid-Gas Foams”, *Journal of Colloid and Interface Science*, Vol. 242, No. 2, pp. 425 – 436, 2001.
- 8 Sattar, M.A., Naser, J., and Brooks, G., “Numerical simulation of slag foaming on bath smelting slag (CaO–SiO₂–Al₂O₃–FeO) with population balance modeling”, *Chemical Engineering Science*, Vol. 107, pp. 165 – 180, 2014.
- 9 Lain, S., Broder, D., Sommerfeld, M., and Goz, M.F., “Modelling hydrodynamics and turbulence in a bubble column using the Euler–Lagrange procedure”, *International Journal of Multiphase Flow*, Vol. 28, pp. 1381 – 1407, 2002.
- 10 OpenFOAM[®], Version 3.0.1, <http://www.openfoam.org>, accessed 2016.
- 11 Bazhlekov, I.B., Chesters, A.K., and van de Vosse, F.N., “The effect of the dispersed to continuous-phase viscosity ratio on film drainage between interacting drops”, *International Journal of Multiphase Flow*, Vol. 26, pp. 445 – 466, 2000.
- 12 Chan, D.Y.C., Klaseboer, E., and Manica, R., “Film drainage and coalescence between deformable drops and bubbles”, *Soft Matter*, Vol. 7, pp. 2235 – 2264, 2011.
- 13 Nguyen, C.T., Gonnermann, H.M., Chen, Y., Huber, C., Maiorano, A.A., Gouldstone, A., and Dufek, J., “Film drainage and the lifetime of bubbles”, *Geochemistry Geophysics Geosystems*, Vol. 14, No. 9, pp. 3616 – 3631, 2013.
- 14 Bale, C.W., Chartrand, P., Deckerov, S.A., Eriksson, G., Hack, K., Mahfoud, R.B., Melançon, J., Pelton, A.D., and Petersen, S., “FactSage Thermochemical Software and Databases”, *Calphad*, Vol. 26, No. 2, pp. 189 – 228, 2002.
- 15 Mills, K.C., Yuan, L., Zhang, G.H. and Chou, K.C., “A Review of the Factors Affecting the Thermophysical Properties of Silicate Slags”, *High Temperature Material Processes*, Vol. 31, No. 4-5, pp. 301 – 321, 2012.
- 16 Mills, K.C., Yuan, L., and Jones, R.T., “Estimating the physical properties of slags”, *Journal of the Southern African Institute of Mining and Metallurgy*, Vol. 111, No. 10, pp. 649 – 658, 2011.
- 17 Oxtoby, O.F., Malan, A.G., and Heyns, J.A., “A computationally efficient 3D finite-volume scheme for violent liquid-gas sloshing”, *Numerical Methods in Fluids*, Vol. 79, No. 6, pp. 306 – 321, 2015.